

Human-centered avalanche susceptibility mapping (H-CASM): shifting the cartographic emphasis of backcountry avalanche susceptibility maps

Lindsey Rotche & Yolanda C. Lin

To cite this article: Lindsey Rotche & Yolanda C. Lin (16 Jan 2024): Human-centered avalanche susceptibility mapping (H-CASM): shifting the cartographic emphasis of backcountry avalanche susceptibility maps, *Cartography and Geographic Information Science*, DOI: [10.1080/15230406.2023.2293886](https://doi.org/10.1080/15230406.2023.2293886)

To link to this article: <https://doi.org/10.1080/15230406.2023.2293886>



Published online: 16 Jan 2024.



Submit your article to this journal 



Article views: 236



View related articles 



View Crossmark data 



Human-centered avalanche susceptibility mapping (H-CASM): shifting the cartographic emphasis of backcountry avalanche susceptibility maps

Lindsey Rotche and Yolanda C. Lin

Geography and Environmental Studies, University of New Mexico, Albuquerque, USA

ABSTRACT

With backcountry winter travel increasing in popularity, the importance of accessible avalanche safety information is crucial. Widely accessible avalanche backcountry maps use slope shading to show where avalanches are likely to start. This paper presents a new methodology called Human-Centered Avalanche Susceptibility Mapping (H-CASM), which shifts the cartographic emphasis of backcountry avalanche maps from the hazard of an avalanche starting in a specific location to risk to a human traveling in the terrain. Utilizing ArcGIS, RAMMS avalanche runout model, and Python, we developed H-CASM as an open-source code to incorporate possible avalanche runouts, terrain traps, and connected slopes while trying to reduce instances of false certainty in visualizations. To provide a more comprehensive representation of susceptible terrain, we integrated aspect, distance to ridges, and vector ruggedness in addition to slope for start zone susceptibility using high-resolution one-meter Digital Elevation Models (DEMs). Avoiding the use of discrete susceptibility categories, we applied continuous gradient shading reducing false certainty in the final visualization. This proof of concept sets a new precedent for the future of backcountry avalanche susceptibility maps.

ARTICLE HISTORY

Received 9 February 2023
Accepted 7 December 2023

KEYWORDS

Avalanche risk; cartographic emphasis; avalanche modeling; backcountry skiing; visualizing risk

Introduction

During the 2020–2021 ski season the United States recorded 37 fatalities and the deadliest week for avalanches in US history (American Avalanche Association, 2021). While avalanches do not affect the same magnitude of people as more publicized natural hazards (floods, earthquakes, fires, etc.), when caught in an avalanche, the fatality rate is high (McClung & Schaerer, 2006). When fully buried under 2 m, an avalanche victim has a 40–45% chance of survival (McClung & Schaerer, 2006). After 15 min of burial, that statistic dramatically reduces (SLF, 2022). With backcountry travel becoming more popular, the importance of accessible avalanche safety information is crucial. Additionally, changing climate is affecting the frequency, location, and types of avalanches occurring due to snow density changes, snow pack changes, irregular weather patterns including changes in wind, rapid temperature fluctuations, and warmer climates (Strapazzon et al., 2021). This increases uncertainty for skiers who have biases based on historic avalanche patterns.

Avalanche susceptibility maps that are widely available for backcountry route planning place emphasis on avalanche start zones and not on risk to the human (e.g.

maps available through CalTopo). More than 90% of avalanche fatalities in the backcountry are triggered by humans (Schmudlach & Köhler, 2016). Most backcountry avalanche fatalities occur because the victim either underestimates the hazard or overestimates their ability to deal with the given hazard (Selcuk, 2013). It is important that we provide backcountry recreationalists a comprehensive visual representation of risk. Current widely available mapping applications do not represent areas at risk connected to or below possible start zones, terrain traps (terrain features that increase risk), or runouts (where the avalanche path flows) (Figure 1).

Additionally, these representations tend to only incorporate slope shading. While slope is the most influential topographic factor affecting avalanche risk, others such as aspect, topographic roughness, and distance to ridges play important roles in avalanche release (McClung & Schaerer, 2006). We present the Senator Beck Basin case study that highlights some of these shortcomings in traditional avalanche mapping.

Senator Beck Basin case study

On January 5, 2019, a group of five students and one instructor were in an American Institute for Avalanche

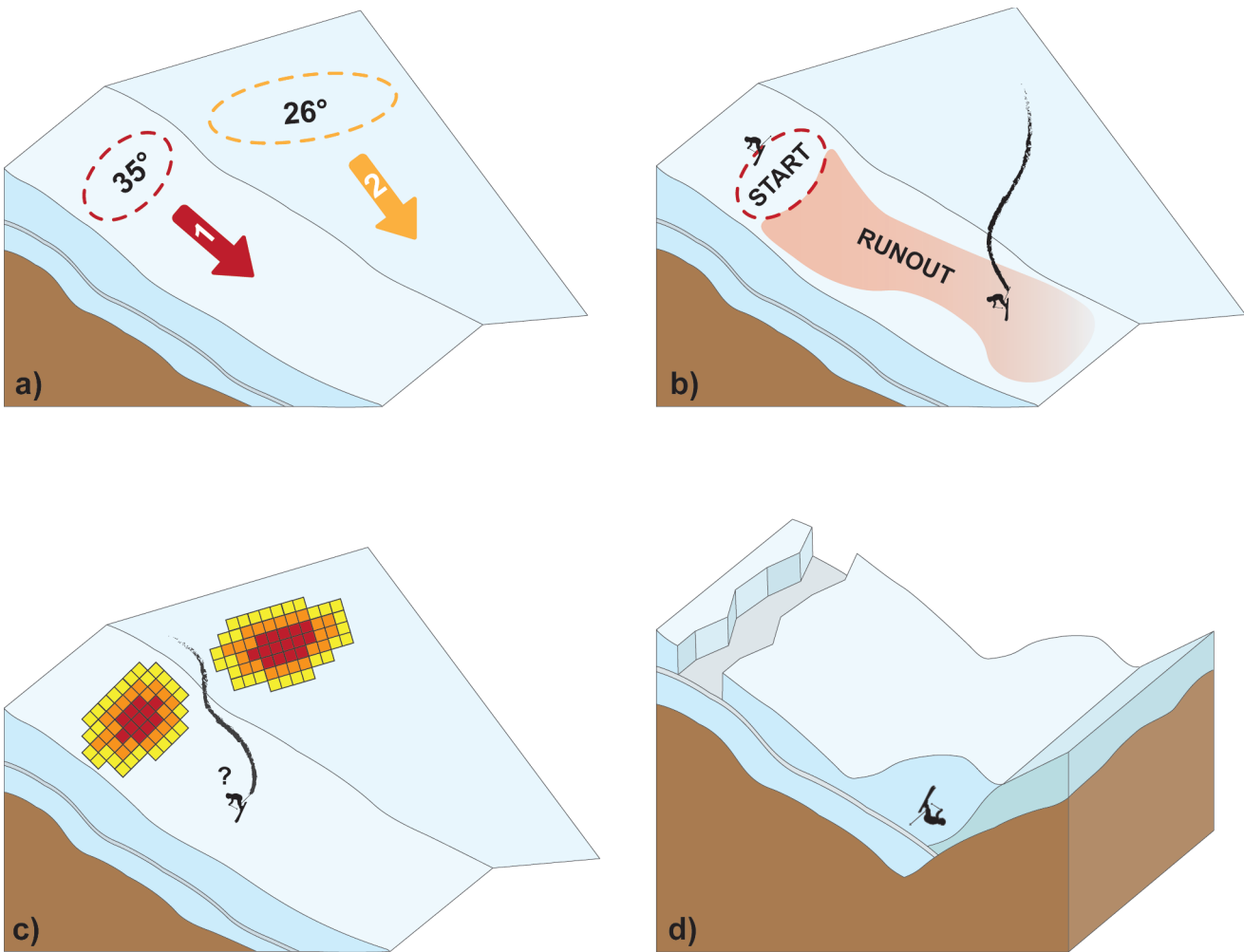


Figure 1. Problems associated with current widely available avalanche susceptibility maps. a) Connected slopes are not visualized or represented; b) Only start zones are shown. As long as a human is in the path of an avalanche, they are still at risk; c) Discrete binning and categories of susceptibility levels (slope values) that imply false certainty; d) Lack of representation of terrain traps which can substantially increase risk.

Research and Education (AIARE) Level 2 class with Silverton Avalanche School (Greene et al., 2019) outside Silverton, Colorado. They were skiing at Senator Beck Basin in Red Mountain Pass (Greene et al., 2019). As this was a level two course, all students had prior avalanche education and it can be assumed that they were experienced backcountry tourers. They used CalTopo, a common digital slope shading map application, to avoid slopes above 30° , the angle widely recognized as where avalanches begin to occur (Greene et al., 2019). On their descent, they planned to follow a narrow terrain feature where the maximum slope was shown to be 29° (Greene et al., 2019). The instructor (Skier One) was the first to enter the slope, followed by Skier Two (Greene et al., 2019). As they were skiing downhill, the rest of the group (Skiers Three through Six) waited at the top maintaining visuals of their group members (Greene et al., 2019).

The skiers at the top (Skiers Three through Six) triggered an avalanche that caught all six people, carrying Skier One and Skier Two a significant distance down-slope (Greene et al., 2019). This initial avalanche then triggered a second avalanche that slid on a connected slope and overlapped the bottom of the first slide (Greene et al., 2019). Skier One was partially buried by the first avalanche, and Skier Two was completely and fatally buried over 2 m deep, covered by both avalanches (Figure 2) (Greene et al., 2019). This fatality stood out to the snow safety world because these skiers were specifically in a class with the goals of understanding, analyzing, and safely navigating through avalanche terrain.

In a review conducted by the Colorado Avalanche Information Center (CAIC) following the accident, the group described using CalTopo to avoid slopes above 30° , and follow a narrow terrain feature where the



Figure 2. Image showing both avalanche paths of the Senator Beck case study and the approximate location of each skier after the avalanches occurred. The initial avalanche pictured in purple was triggered by skiers 3–6 and caught all six skiers. The second avalanche pictured in blue was remotely triggered on a connected slope by the first avalanche. Skier 2 was fatally buried by both avalanches. Picture adapted from Greene et al. (2019) and used with permission from CAIC.

maximum slope was shown to be 29° (Greene et al., 2019). Their GPS tracks show they did follow this planned route (Figure 3). When CAIC employees visited the site, they measured angles ranging from 32° to 34° in this location (Greene et al., 2019). With the present avalanche danger at the time, this turned out to be a fatal discrepancy.

Slope layers are created by comparing the elevation of a neighborhood of pixels in a DEM. The lower the resolution of the DEM, the lower the accuracy of the slope layer. CAIC compared the slope values created from the 10 m DEM CalTopo was using, to a slope layer created from a 3 m DEM. The slope layer created from the 3 m DEM shows the group was well within avalanche terrain (Figure 3).

This fatal event provides several relevant lessons that inspired the following research:

- (1) Maps are a representation of reality. There will always be discrepancies and uncertainties between what the map shows and Earth's surface.
- (2) Connected slopes and overlapping runouts are important aspects of risk to someone traveling in avalanche terrain.
- (3) While it should be stressed that maps are one tool in a quiver of sources of information, it is important that map makers provide the best available data for decision-making.

Developments in avalanche susceptibility mapping

Avalanches occur because of complex interactions between topographic, snowpack, and meteorological conditions (Laute & Beylich, 2014). A slope avalanche due to additional loading (human or natural) or rapid

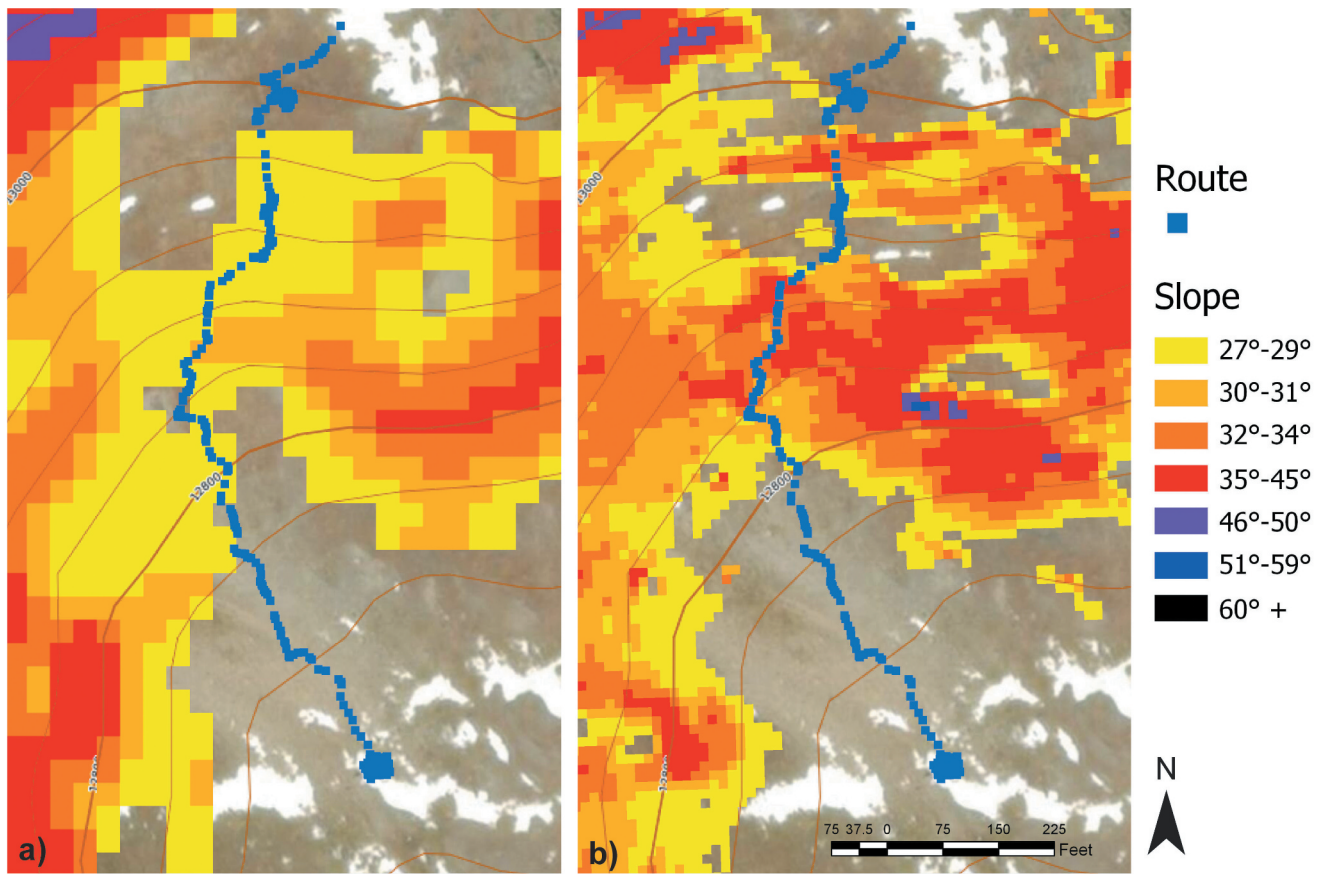


Figure 3. Maps comparing slope shading created from the a) 10 m DEM that CalTopo was using during the time of the Senator Beck case study versus b) slope shading created from a 3 m DEM. When planning their route, the group used the 10 m DEM, attempting to avoid slopes above 30° (the slope value at which avalanche danger is widely considered to dramatically increase). The group's track is shown in blue. While this route appears to stay below 30° with the 10 m resolution layer, when compared with the 3 m resolution layer, it is apparent the group was well within avalanche terrain. Image adapted from Greene et al. (2019) and used with permission from CAIC.

increase in warming creating its own source of lubrication (Bühler et al., 2013) on angles generally ranging from 30° to 45° (McClung & Schaerer, 2006). There are two main types of avalanches that threaten backcountry recreationalists: loose snow and slab. Loose snow avalanches tend to start near the surface at a single point, and usually only involve surface snow (McClung & Schaerer, 2006). Slab avalanches are often much more dangerous, initiate by a failure of a weak layer within the snowpack, and involve a block of snow that flows downhill and immediately cements into a very high-density layer when settled (McClung & Schaerer, 2006). This study focuses on slab avalanches as they pose the highest risk to backcountry travelers including skiers, snowboarders, snowmobilers, and snowshoers.

Geographic Information Systems (GIS) have emerged as one of the frontrunners in communicating avalanche danger. While slope is identified as the most dominant topographic variable controlling avalanche release, modeling has been found to be more

accurate with the inclusion of multiple factors (Table 1) (Ghinoi & Chung, 2005; Pisticci & Notarnicola, 2013).

When referencing (Table 1) it becomes apparent that curvature is a commonly used parameter that this study did not include. Curvature of a slope is one of the less standardized and agreed upon factors in topographic modeling of avalanche susceptibility. There is disagreement among studies about which type of curvature is most susceptible to avalanche release, stated importance, and appropriate DEM resolution. The majority of studies put a low weight on curvature (Kim & Park, 2019; Suk & Klimánek, 2011), however Maggioni and Gruber (2003) rank curvature as one of the most influential factors. Because of the many inconsistencies within the literature, we excluded it from this study.

Moving beyond basic start zone susceptibility, Maggioni and Gruber (2003) were the first to use GIS to identify and delineate avalanche release areas. Christen et al. (2010) developed RAMMS, currently

Table 1. Table of past studies and the topographic parameters they used to model avalanche start zone susceptibility.

Date	Authors	Slope	Aspect	Curvature	Vegetation/ land cover	Roughness/ Ruggedness	Distance to ridges	Elevation	Other
2022	This Study
2022	Bühler et al.
2021	Sykes et al.
2020	Larsen et al.
2020	Soteres et al.
2020	Yariyan et al.
2019	Choubin et al.
2019	Chymyrov et al.
2019	Gusain et al.
2019	Kim and Park
2019	Kumar et al.
2019	Tariq et al.
2018	Bergua et al.
2018	Bühler et al.
2018	Harvey et al.
2018	Kumar et al.
2017	Aydin and Eker
2017	Parshad et al.
2016	Kumar et al.
2016	Schmudlach and Köhler
2016	Veitinger et al.
2015	Mohammed et al.
2014	Cía et al.
2014	Laute and Beylich
2014	Ozsahin and Kaymaz
2013	Bühler et al
2013	Pistocchi and Notarnicola
2013	Selcuk
2012	Andres and Cía
2011	Barbolini et al.
2011	Suk and Kilmanek
2005	Ghinoi and Chung
2003	Gruber and Sarderman
2003	Maggioni and Gruber
Total		34	20	25	16	14	6	16	10

the most widely used and validated avalanche runout simulation model (Bühler et al., 2022). RAMMS is a numerical, three-dimensional flow simulation model (Christen et al., 2010). Required inputs are a DEM, release area polygon, fracture depth, and optionally a binary vegetation layer (Christen et al., 2010). Friction parameters and return periods are specified within the model, and after running, it outputs max flow height, deposition, and max pressure rasters (Christen et al., 2010). Veitinger et al. (2016) introduced the concept of a wind shelter index, varying roughness with snow depth, and utilized fuzzy logic to account for uncertainty, an important step in incorporating the effects of changing snow conditions and uncertainty. Bühler et al. (2018) improved automated start zone delineation creating a foundation for automated large-scale avalanche hazard mapping.

Few studies have been conducted for the intention of backcountry ski travel (Dewali et al., 2014; Harvey et al., 2018; Schmudlach & Köhler, 2016; Vontobel et al., 2013). Dewali et al. (2014) created a navigational GPS app based off historic avalanche

paths to facilitate travel in avalanche terrain, providing status alerts of “safe,” “near path,” or “in path.” Vontobel et al. (2013) used GIS to analyze terrain characteristics of start zones of small and medium human triggered avalanches, providing valuable insight for future mapping. Schmudlach and Köhler (2016) and Harvey et al. (2018) were the first to introduce the concept of more comprehensive automated avalanche susceptibility maps. Schmudlach and Köhler (2016) automated Avalanche Terrain Exposure Scale (ATES) mapping, categorizing the terrain into “simple,” “challenging,” and “complex.” Harvey et al. (2018) used GIS to classify terrain of avalanches that typically threaten backcountry recreationalists, modeling potential release areas (with slope, fold, and curvature), possibility for remote triggering, runouts, and extreme terrain with high fall potential. Harvey et al. (2018) work relates most similarly to this project, however, we introduce a new, more accessible method for start zone delineation, use different methodology for start zone susceptibility and terrain traps, rely less on specific RAMMS outputs, and use different cartographic strategies.

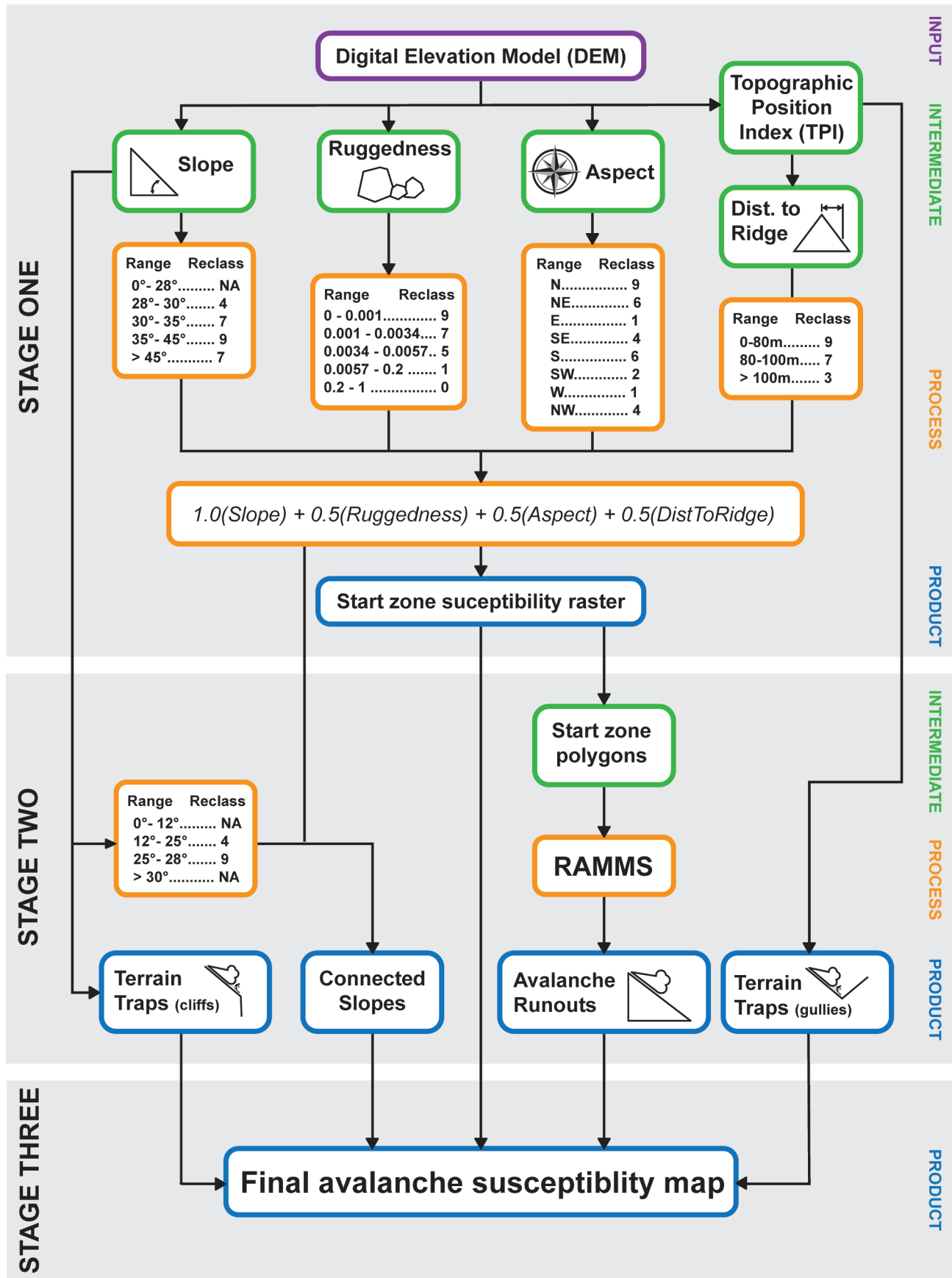


Figure 4. Flowchart for new methodology proposed in this paper (H-CASM) to create human-centered avalanche susceptibility maps. This methodology is broken into three stages: the creation of the start zone susceptibility raster (Stage One); the creation of terrain traps, potential runouts, and connected slopes (Stage Two); and the incorporation all layers into a final avalanche susceptibility map (Stage Three). Purple represents outside inputs, green represents intermediate layers, gold represents processing steps, and blue represents products.

Methods

It is widely understood that the factors influencing avalanche hazard can be divided into three groups: topographic, metrological, and snowpack. Because snowpack and meteorological data are so dynamic and the information can be less accessible, many studies focus solely on static terrain parameters, stating they have great influence on meteorological and snowpack conditions (Bühler et al., 2013; Pistocchi & Notarnicola, 2013). We followed this concept by only including topographically based layers.

Our methodology, Human-Centered Avalanche Susceptibility Mapping (H-CASM), includes representing more detailed possible start zones, runouts, connected slopes, and terrain traps compared to traditional avalanche susceptibility slope shading maps. Requirements for the current H-CASM methodology include a DEM, GIS software, and an avalanche runout model. The implementation and codes discussed in this paper utilize Python 2.7, ArcMap 10.7 GIS software, and RAMMS avalanche runout model. Optionally, aspect susceptibility weighting and vector ruggedness can be changed within the script to customize it for a given study area. We used one-meter resolution DEMs from United States Geologic Survey's (USGS) 3DEP program (USGS, 2022). From these DEMs, slope, vector ruggedness measure (VRM), aspect, and topographic position index (TPI) layers are created (Figure 4). Using the TPI layer, a ridges layer, and then a distance to ridges layer is created. Slope, VRM, aspect, and distance to ridges are reclassified on a scale of 0–9 (Kumar et al., 2018; Mohammed et al., 2015; Parshad et al., 2017) or NULL according to their influence on avalanche release. Layers are then weighted and added together. This process is done for slope angles above 28° to create a start zone susceptibility raster and again for angles from 12° to 28° to create a connected slope susceptibility layer. Start zone polygons are created using a grid of points to be input into RAMMS to calculate avalanche runouts. Terrain trap layers are created by extracting gullies from the TPI layer and slope angles above 50° from the slopes layer. All layers are then compiled into a final avalanche susceptibility map.

It should be stressed that while our data is based on an extensive literature review and expert judgment, precise weights and reclassification values were not the goal of this study. Our goal was to create a framework and new methodology for H-CASM. In the future, H-CASM can be adapted to incorporate more precise parameters to further decrease uncertainty.

The study area for this project is a portion of Red Mountain Pass near Silverton, CO including Senator Beck Basin, the location of the case study discussed above (Figure 5). Silverton, CO, home of Silverton Avalanche School and Silverton Ski Area, lies at 9,318 ft surrounded by mountains popular for winter backcountry travel (Silverton Chamber of Commerce, 2022). Red Mountain Pass is a popular backcountry destination in this area, and a common location for Silverton Avalanche School classes. It is just above 11,000 ft in elevation.

Start susceptibility raster

Multi-Decision Criteria Analysis methodology was used to create the avalanche start zone susceptibility raster. This is a commonly used method in GIS and avalanche susceptibility mapping that ranks multiple criteria based off influence (Cia et al., 2014; Mohammed et al., 2015; Parshad et al., 2017; Selcuk, 2013). An open-access python code was developed to perform this analysis (Rotche, 2022). The only required input data is a DEM. The code creates slope, aspect, distance to ridges, and vector ruggedness layers. The Analytical Hierarchy Process was used to determine reclassification of ranges within each parameter and overall rankings. Applying expert knowledge, ranges from 0 to 9 or NULL were used to rank categories on their degree of influence toward avalanche susceptibility (Kumar et al., 2018; Mohammed et al., 2015; Parshad et al., 2017). The higher the ranking, the more likely the category is to influence avalanche release.

Slope

Slope is the most influential topographic parameter that impacts avalanche release susceptibility (McClung & Schaefer, 2006). Avalanches mainly occur on slopes ranging from 30° to 50° (Tariq et al., 2019) and are most likely from 35° to 45° (McClung & Schaefer, 2006). While these are not strict limits, normally the gravitational force is not strong enough on lower inclines, and steeper inclines cannot accumulate enough snow to form a large avalanche (McClung & Schaefer, 2006). Soteres et al. (2020) used only slope as a main parameter, with aspect and snowpack permanence as enhancer factors. To maintain the strong influence of slope on avalanche release, this study followed a similar outline using slope to define susceptible locations for start zones and aspect, distance to ridges, and vector ruggedness as enhancer factors. To

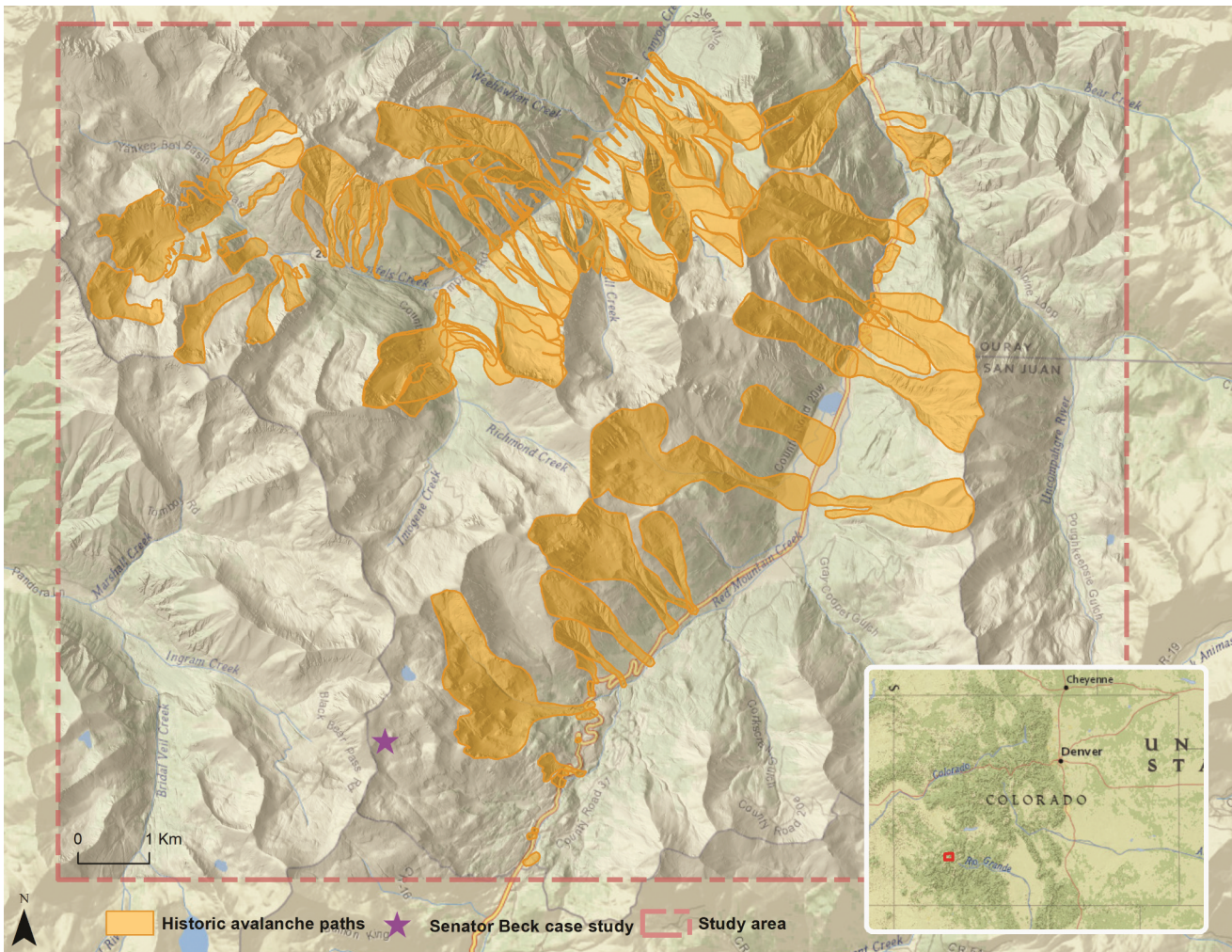


Figure 5. Red Mountain Pass study area (shown in red): a popular winter backcountry destination in southern Colorado including the location of the Senator Beck case study (purple star) and historic avalanche paths (orange polygons) from CAIC.

Table 2. Slope reclassification for start zone susceptibility.

Slope	Reclassification	Source
0° – 28°	NULL	Veitinger et al. (2016)
28° – 30°	4	Tariq et al. (2019)
30° – 35°	7	Temper (2008)
35° – 45°	9	McClung and Schaerer (2006)
>45°	7	McClung and Schaerer (2006)

create the start zone susceptibility raster, only slopes 28° and higher were considered (Veitinger et al., 2016) (Table 2).

Aspect

The aspect of a slope has two major effects on avalanche susceptibility: solar insolation and wind effect (McClung & Schaerer, 2006). In the winter in the northern hemisphere, it is generally understood that the northern/shadier aspects are less stable,

while in the spring, the southern/sunnier aspects are less stable (Suk & Klimánek, 2011). Leesides of ridges tend to have increased snow accumulation due to wind effect and are therefore more susceptible to avalanche initiation (McClung & Schaerer, 2006). Highest risk aspects are dependent on the study area and can vary due to wind direction from a specific storm, season, and temperature. Because of this, aspect is one of the more dynamic and study area dependent topographic parameters. We recommend that this be included as a dynamic variable based off local weather and avalanche forecast in future implementation. To provide the framework, we use weather station data (CAIC, 2022) of dominant wind direction (Figure 6) for the study site to create the weighting system of the relevant susceptible aspects (Table 3 and Figure 7). For our Red Mountain Pass study area, dominant wind direction was from the south. Winds from the

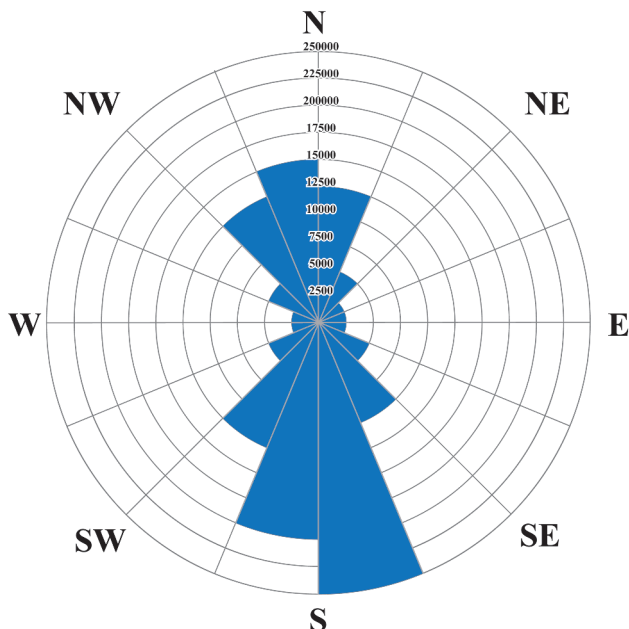


Figure 6. Peak wind direction for Abrams station located near Red Mountain Pass, CO. Intervals represent number of records in 2,500 record increments.

Table 3. Aspect reclassification for start zone and connected slope susceptibility. This data is represented graphically in Figure 7.

Aspect	Reclassification
N	9
NE	6
E	1
SE	4
S	6
SW	2
W	1
NW	4

north were next most frequent, with eastern and westward winds least likely. This correlates to northern sides of ridges being the most susceptible to wind loading, and southern sides being the next most susceptible.

Vector ruggedness

Rough features can anchor snowpack (McClung & Schaerer, 2006) while smooth bedrock can act as a sliding surface. Some studies calculate this parameter using Topographic Roughness Index (TRI) (Chyhyrov et al., 2019; Yariyan et al., 2020), while others use Vector Ruggedness Measure (VRM) (Aydin & Eker, 2017; Bühler et al., 2013). TRI is strongly correlated with slope, while VRM is independent (Sappington et al., 2007). In their study, Sappington et al. (2007) found that TRI is so linked to slope that it is not possible to receive low topographic roughness values (i.e. smooth surface) with steep slope measurements. Because the

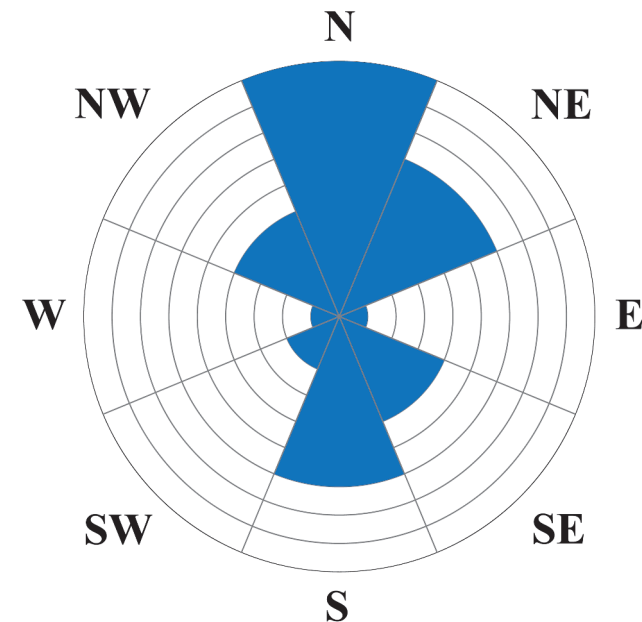


Figure 7. Graphical chart of aspect reclassification for start zone and connected slope susceptibility. This data is represented numerically in Table 3.

terrain being analyzed in this study is intrinsically steep, VRM serves as a more appropriate measure. While VRM is a dynamic variable based off snow depth, we create a framework for static numbers that can be adapted in the future to include dynamic updates based on measured snow depths using similar methodology to Veitinger et al. (2016). Values from 0 to 0.001 represent the smoothest and most susceptible terrain (Veitinger et al., 2016). Vontobel et al. (2013) found that 50% of their start zones had VRM values less than 0.0034, and 75% of them were less than 0.0057. Avalanches are considered “not to occur” with VRM values greater than 0.02 (Veitinger et al., 2016). Reclassification values were applied using those criteria (Table 4).

Distance to ridge

Multiple studies place distance to ridges as a highly influential topographic parameter on avalanche release (Gruber & Sardemann, 2003; Kim & Park, 2019; Maggioni & Gruber, 2003). This is mainly a factor of wind transport and cornice formation as well as tension

Table 4. Vector ruggedness reclassification for start zone and connected slope susceptibility.

VRM	Reclassification	Source
0–0.001	9	Veitinger et al. (2016)
0.00–0.0034	7	Vontobel et al. (2013)
0.0034–0.0057	5	Vontobel et al. (2013)
0.0057–0.2	1	Veitinger et al. (2016)
>0.2	0	Veitinger et al. (2016)

Table 5. Distance to ridge reclassification for start zone and connected slope susceptibility.

Distance to Ridge (meters)	Reclassification	Source
0–80	9	Gruber and Sardemann (2003)
80–100	7	Pistocchi and Notarnicola (2013)
>100	3	Pistocchi and Notarnicola (2013)

points. Gruber and Sardemann (2003) state an avalanche is most likely to occur within 80 m of a ridge. Pistocchi and Notarnicola (2013) state avalanches are most likely to occur within 100 m of a ridge. Reclassification values were applied to distance categories accordingly (Table 5).

Total

Each layer was reclassified according to their influence on avalanche start susceptibility. Higher numbers represent ranges more conducive to avalanche release. After reclassification, layers were weighted and added together into a final susceptibility raster with the following equation:

$$\text{Susceptibility} = (1.0)\text{Slope} + (0.5)\text{Ruggedness} + (0.5)\text{DistToRidge} + (0.5)\text{Aspect}$$

Not only was slope used as the determining factor for start zones (only slopes >28° were considered), but it was also weighted the highest in the susceptibility equation as it has the greatest influence on avalanche initiation (McClung & Schaefer, 2006). Ruggedness, distance to ridges, and aspect were all weighted by 0.5 because while they influence avalanche release susceptibility, they are only enhancer factors, not determining factors. Their weights were kept even and generically 0.5 because literature does not agree on which parameters are most influential. The goal of this generic weighting is to avoid the representation of false certainty within our equation. In future research, these weights can easily be changed and adapted within the methodology.

Connected slopes

When on a slope that has an angle that is less than what is typically referred to as avalanche terrain, it is still possible to cause a remote trigger of a connected steeper slope (Temper, 2008). It is also possible that if a steeper slope slides adjacent to a connected slope, it can cause that less steep area to slide as well (Temper, 2008). Referencing lower probability slope ranges for avalanche initiation, literature on avalanche mapping

Table 6. Slope reclassification for the connected slope susceptibility raster.

Slope	Reclassification	Source
0° – 12°	NULL	Kumar et al. (2016)
12° – 25°	4	Mohammed et al. (2015)
25° – 28°	9	Yariyan et al. (2020)
>28°	NULL	Veitinger et al. (2016)

generally recognizes 12° as the minimum possible slope for a slide (Kumar et al., 2019; Mohammed et al., 2015; Parshad et al., 2017). A 25° inclination is generally agreed to be the point where avalanche danger becomes more likely (McClung & Schaefer, 2006; Yariyan et al., 2020). In this study, we define connected slopes as locations that fall within 12°–28°. While unlikely to release on their own, these slopes have the potential to release if an adjacent slope avalanches. A connected slopes susceptibility layer was created using the same method for the start zone susceptibility layer except for slopes from 12° to 28° (Table 6).

Runouts

RAMMS (Christen et al., 2010), the most widely applied, tested, and validated avalanche runout model (Bühler et al., 2022) was used for this project. To run the model, start zone polygons had to be created. This free and open-source python code is available by the authors via GitHub (Rotche, 2022). Average start zone area of historic paths (CAIC, 2021) was calculated as 80,989 m² based off the area of the highest elevated third (Bühler et al., 2013) of each path. A simple conversion ($80,989 = \pi r^2$) was used to determine 160 m as the radius of a circle with equivalent area. This value was used to create a grid of points within susceptible start zone locations spaced 160 m apart. Each point was buffered to create a circle with the specified radius (160 m). Buffer distance and grid spacing are the same number to ensure enough overlap, but also to maintain easy adaptability for future changes in start zone size. Circles were then clipped to the start zone susceptibility layer (locations greater than 28°). Ridges were erased from the start polygons to avoid release areas that spanned overtop a ridge. Finally, polygons with an area less than 1000 m² were deleted to avoid very low probability release areas and create the final vector files for start zones (Bühler et al., 2022). All start zones were then run through RAMMS using a 5 m DEM to determine avalanche runouts. A fracture depth of 61 cm for the start zones was chosen based off average max crown height of historic avalanches in Colorado (CAIC, 2021). A 100-year return period for

“large” avalanches and no vegetation layer was used to determine friction values for probable maximum runouts for the start zones.

Terrain traps

Terrain traps are terrain features that amplify consequences of being caught in an avalanche (Temper, 2008). For this project terrain traps were considered to be gullies and highly concave features, and extreme steep terrain and cliffs. Gullies can trap avalanche debris creating a much deeper deposition zone and therefore a much deeper victim burial with a lower chance of survival (Temper, 2008). These features can also funnel a human into an avalanche path making their likelihood of getting caught higher, or funnel avalanche routes into the same path (Temper, 2008). Gullies and highly concave features were specified as anywhere with a TPI value less than the negative standard deviation (Weiss, 2001). If a person is caught in an avalanche above a drop-off, there is a high likelihood that person will be swept over the extreme terrain, increasing the possibility of serious injury or death (McClung & Schaefer,

2006). Cliffs and extreme terrain were specified as anywhere with a slope greater than 50° (Harvey et al., 2018).

Results

Start susceptibility, connected slope susceptibility, potential runouts, and terrain traps were all layered in the final map (Figures 8 and 9). This can be compared to traditional slope shading methodology for the same area derived from the same DEM (Figure 9).

Color has long been recognized as a very important aspect in communication through cartography (Robinson & Sale, 1969) and is arguably one of the most important elements (Sun, 2015). Hoarau (2011) stresses that for a map to make sense, a chosen color scheme must be consistent with the relationship it represents. For this reasoning, we retained a similar color range for start zone susceptibility and connected slopes to traditional slope shading maps. Our goal was to maintain consistency in perception of areas of higher susceptibility across methodologies. Start zone susceptibility is represented in

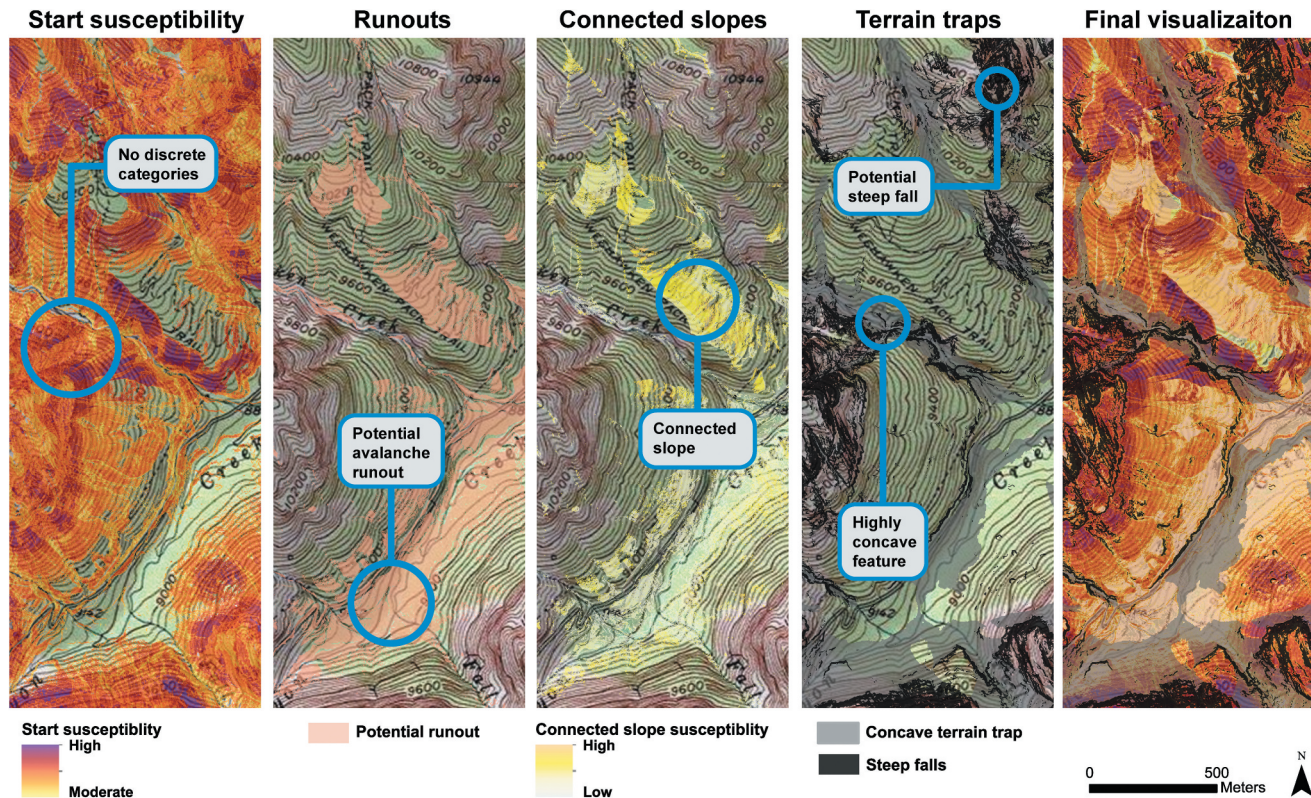
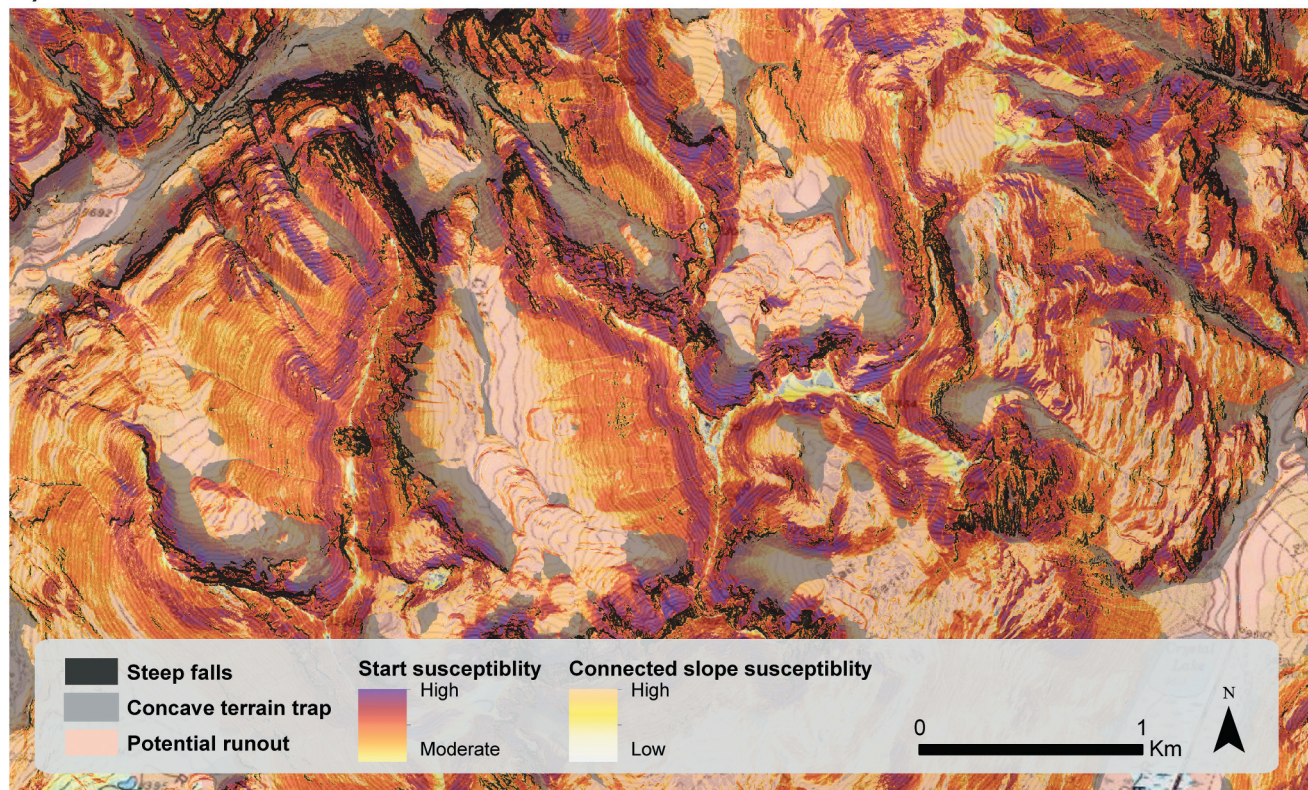


Figure 8. Individual symbolization and explanation of layers in new human-centered avalanche mapping methodology (H-CASM) for a portion of Red Mountain Pass, CO. The final pane (“Final visualization”) shows the full visualization used in H-CASM methodology, a compilation of all of the layers.

a)



b)

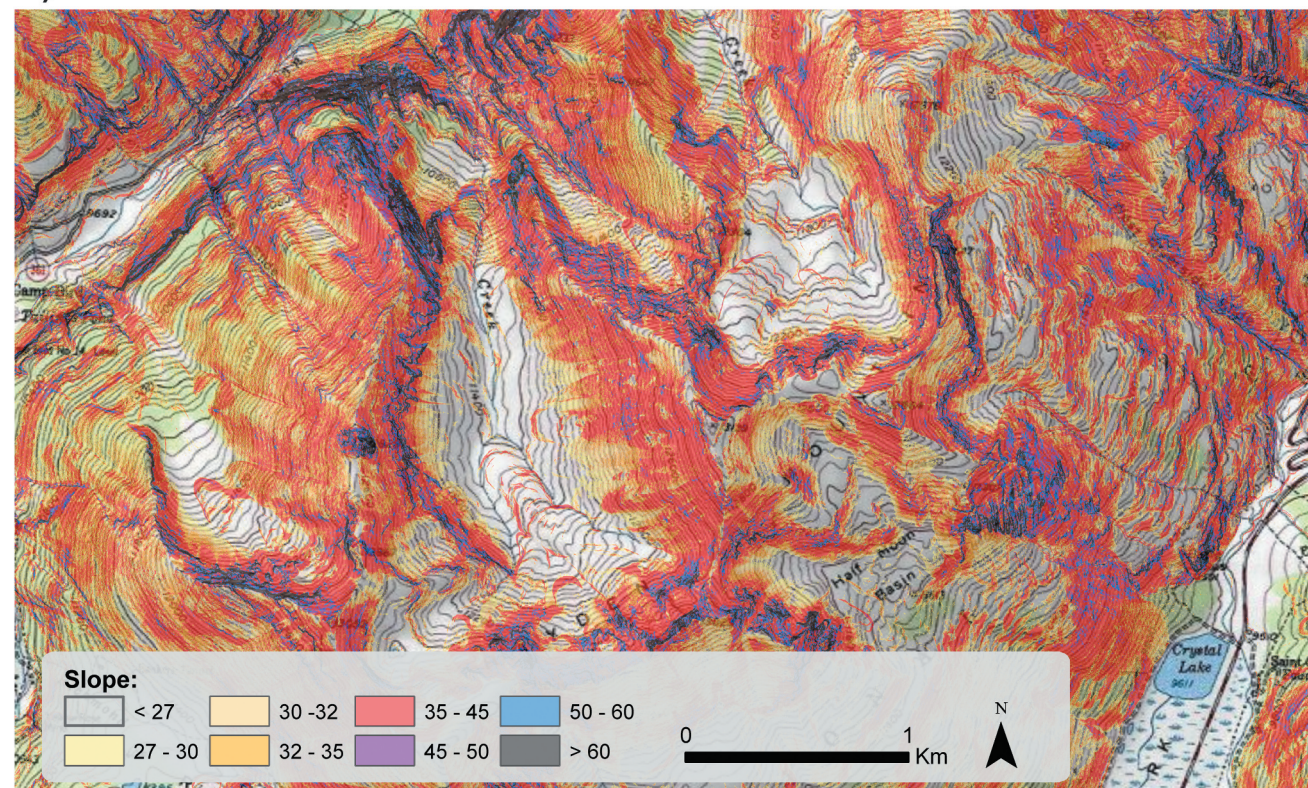


Figure 9. Comparison of a) the new human-centered avalanche susceptibility mapping methodology (H-CASM) proposed in this paper and b) traditional slope shading methodology. H-CASM includes start zone susceptibility (purple to yellow), potential runouts (light red-orange), connected slope susceptibility (light orange to clear), steep falls (black), and concave terrain traps (gray). When comparing maps, notice the blank areas in the traditional methodology that may imply a false sense of "safety," and the discrete binning of categories that imply a false sense of certainty. Both maps represent the same portion of Red Mountain Pass in Southern Colorado, were created with the same DEMs, and are displayed with a USGS topographic map background.



a color gradient ranging from purple to dark red to dark orange to yellow. Connected slope susceptibility is visualized with a dark yellow to no color gradient. The color ranges of connected slopes and start susceptibility overlap, because while in this methodology they were separated distinctly at 28°, in reality, the determination of a start zone vs connected slope is much more uncertain. Lower susceptibility start zones are not necessarily substantially different than highly susceptible connected slopes. For features that are not displayed in traditional maps (terrain traps and runouts) we followed the logic that similar items should be symbolized similarly (Raisz, 1962; Sun, 2015). As runouts are part of the avalanche itself, we symbolized them in light red-orange, following the warm color gradients of start zones and connected slopes. Representing areas of higher consequence, but not part of the avalanche itself, we symbolized terrain traps in dark gray for gullies and black for steep falls, indicating areas that should be avoided.

Kunz et al. (2011) stress most hazard maps falsely imply absolute certainty with solid borders of hazard zones even though experts agree that these borders are uncertain. Following this logic, we employ a gradient color bar for start zone and connected slope susceptibility in contrast to the traditional methodology of categorical breakpoints. This shows a more continuous susceptibility layer, reducing instances of false certainty. It also reduces some of the bias and uncertainty involved in choosing discrete classes (Brassel & Utano, 1979).

Each layer is displayed with some transparency to show the underlying basemap and influence of other layers. The top most layers are terrain traps, visualized at 45% transparency for gullies and 20% transparency for steep falls. As steep falls represent cliffs, these are locations of clearly high risk regardless of other factors, making importance of underlying layers negligible. The start susceptibility layer is visualized at 40% transparency. Runouts are visualized with at 55% transparency. Connected slopes are visualized at 40% transparency, below runouts. The yellow connected slopes below light red-orange runouts allow the colors to build upon each other. If a connected slope and a runout are overlapping, the color will be darker and more opaque, implying higher susceptibility. Runouts were determined higher risk than slopes ranging from 12° to 28° (connected slopes) and were therefore placed on top with greater emphasis. It is suggested that these layers be incorporated in a web application or similar product with the ability to turn them on and off for customization by the user.

Validation

A common issue in creating avalanche susceptibility maps is the lack of historic avalanche data (Bühler et al., 2022). Having an incomplete set tells us where certain avalanches have occurred, but not where all avalanches can occur (Suk & Klimánek, 2011). If there is no path data for a location, this does not mean an avalanche has not, or cannot, occurred in that location, but that it has not been recorded. Due to these difficulties, it is not uncommon to perform qualitative visual analyses or minimal validation (Barbolini et al., 2011; Bergua et al., 2018; Bühler et al., 2022; Mohammed et al., 2015; Soteres et al., 2020; Sykes et al., 2021).

We obtained the most detailed and complete dataset available from CAIC (2021) (Figure 10). The majority of paths that have been mapped are those of interest to the Department of Transportation, and therefore lie along roads and not at popular backcountry ski locations. All 117 historic paths in the database for our study area are along a road. Although incomplete, we overlaid all existing paths on our maps to visually assess for accuracy. Based on this visual inspection, most paths aligned well within the susceptibility map. Start zones are pictured accurately in shades of red, terrain traps correctly identified areas where the path is funneled, and runouts are covered. Figures 10 and 11 show five example paths. Paths A, B, and C provide examples of good alignment between the historic path and the H-CASM symbology (Figure 11). There are 2 of the 117 runouts (D and E) that did not have their full extent symbolized (Figure 11). The uncovered extent is over a very flat area and therefore exemplifies an extreme scenario.

Application of H-CASM to Senator Beck case study

After creating our methodology, H-CASM, we applied it to the Upper Senator Beck case study discussed in this paper (Figures 12 and 13). We also compared the same area to traditional slope shading methodology derived from the same DEM (Figure 13). Not only does our map show clear start susceptibility along the route, but it also shows a large area covered by a concave terrain trap. While this terrain trap does not represent a gully, what is typically considered a concave terrain trap, it shows where avalanches will be funneled, and therefore where paths may overlap. While we do not know the state of the victim's burial after the first avalanche in this case study, we do know that the victim ultimately ended up being covered by both runouts, making burial much deeper and extrication much harder. When buried greater than 2 m deep, survival rates are very low

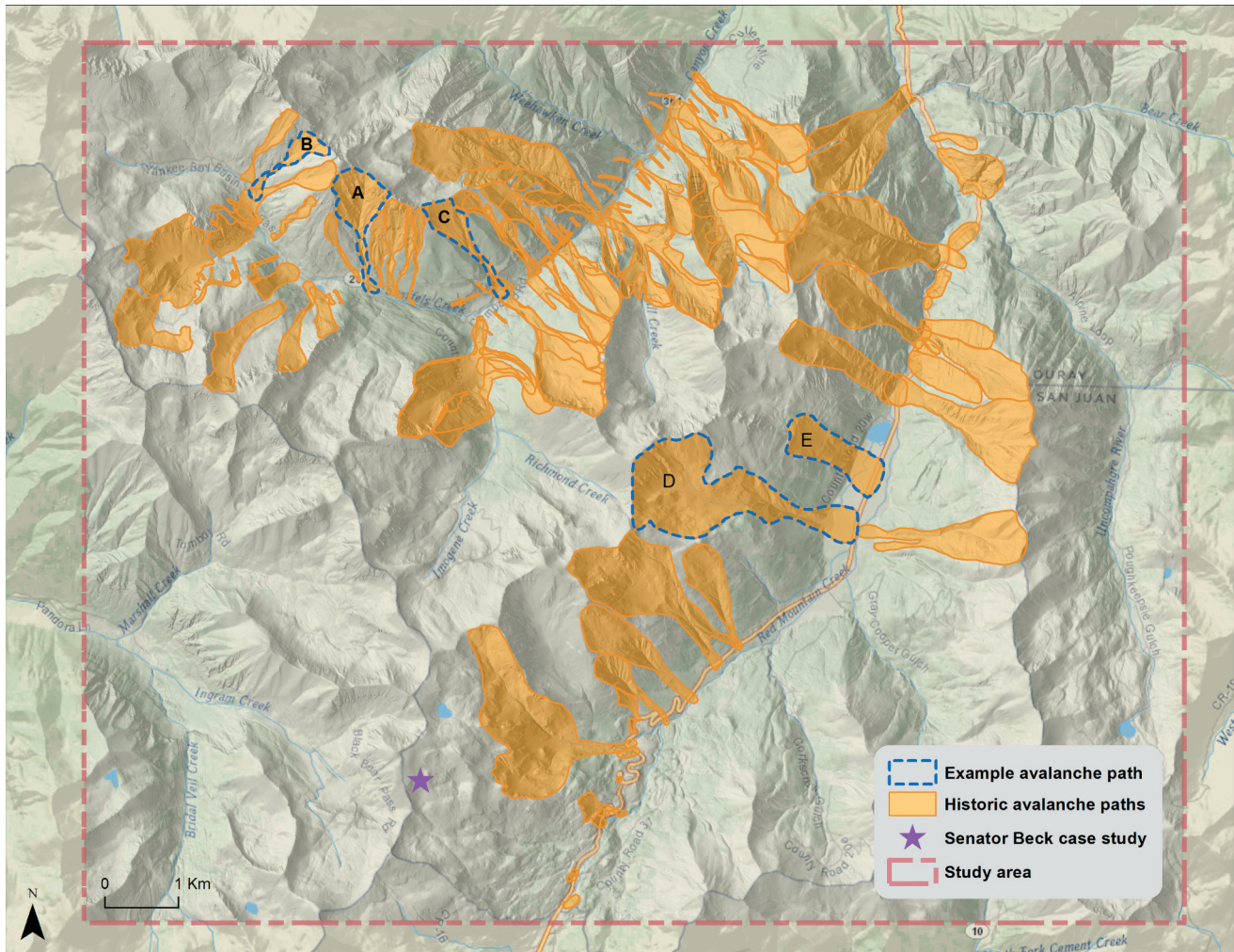


Figure 10. All historic avalanche paths obtained and used for validation in this study area are represented in orange. Example historic paths shown with H-CASM methodology in Figure 11 are shown with a dashed blue outline. The Senator Beck case study is shown with a purple star, and the total study area is shown with a red dashed line.

(McClung & Schaefer, 2006). This individual was buried over 2 m deep, and it took about 50 min to completely free him (Greene et al., 2019). He had no pulse on extrication (Greene et al., 2019).

Discussion

The goal of this project was to provide a methodology for, and introduction of, a new concept to shift how we look at avalanche hazard maps. This study sets a foundation for shifting backcountry avalanche mapping emphasis to focus on human needs. The maps developed in this study provide a visualization of overall avalanche susceptibility to someone traveling in the terrain, in contrast to current widely available maps that only show the hazard of where an avalanche can start. We incorporated terrain traps, connected slopes, and possible runout zones in addition to start

susceptibility. Within start susceptibility, we included not only slope but also ruggedness, distance to ridges, and aspect. We also utilized a gradient shading method instead of commonly used categorical breakpoints to reduce a false sense of certainty. It is important to note here that H-CASM is human-centered as it is a tool to help aid in human decision-making, while solely user-centered tools focus only on reducing technological problems and creating easier to use products (Gasson, 2003).

A common criticism of this methodology may be that H-CASM provides “too much information” and “everywhere appears susceptible.” We carefully considered this when designing these maps. Ultimately, we decided that the best approach was to provide start susceptibility, connected slopes susceptibility, and terrain trap layers, with the intent this methodology be incorporated into an interactive digital application where individual

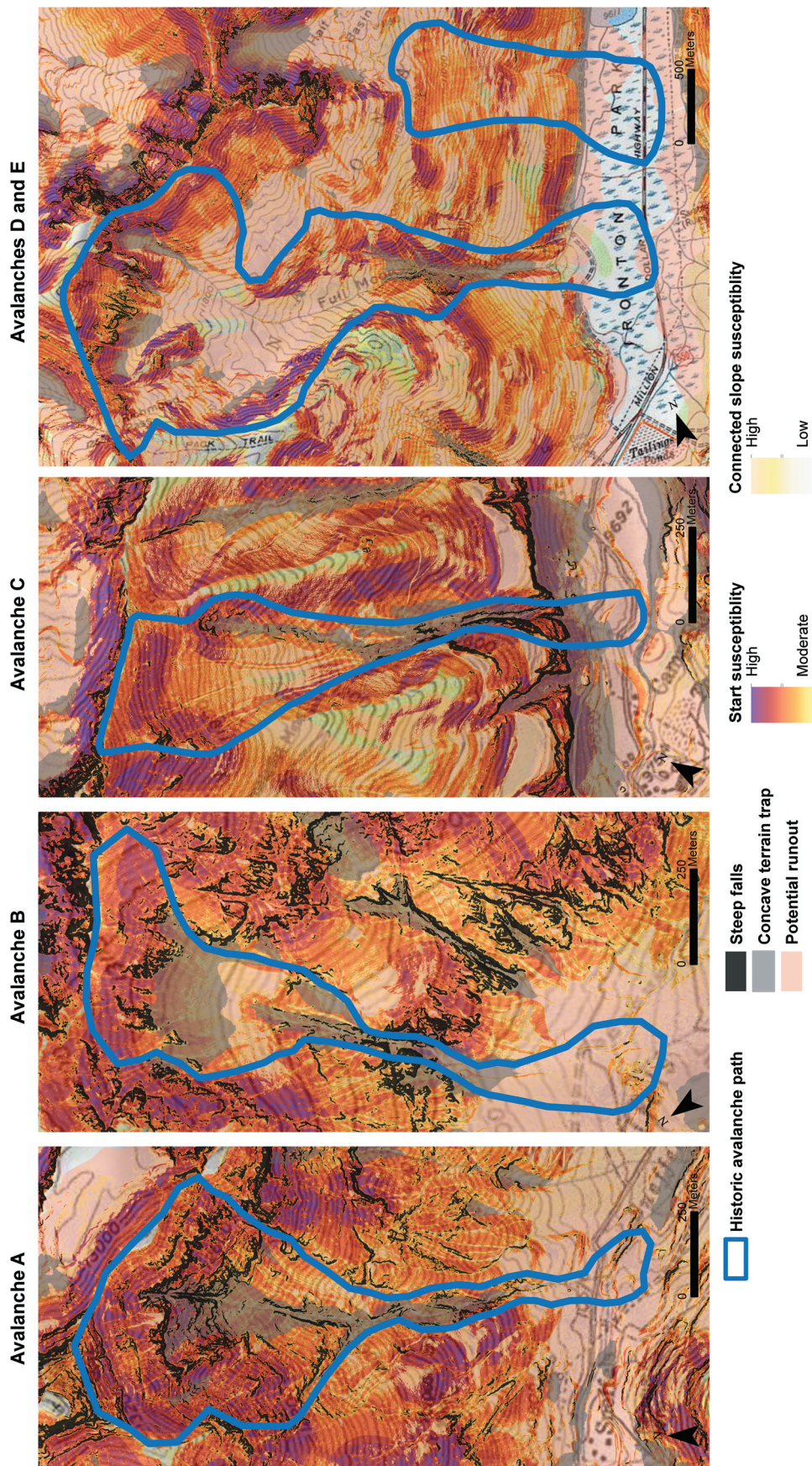


Figure 11. Historic avalanche paths overlaid on H-CASM methodology to show alignment of symbology. Paths A, B, and C show good alignment. Note the top of the paths are shaded with high start susceptibility coloration, concave terrain traps show where the path is funneled, and runouts are completely covered with potential runoff shading. Paths D and E are the only two of 117 paths in our validation database whose extent was not completely covered by “potential runoff” in the H-CASM map. It is important to note that these historic paths are extreme scenarios related to the Colorado Department of Transportation and potential road blockages and damage.

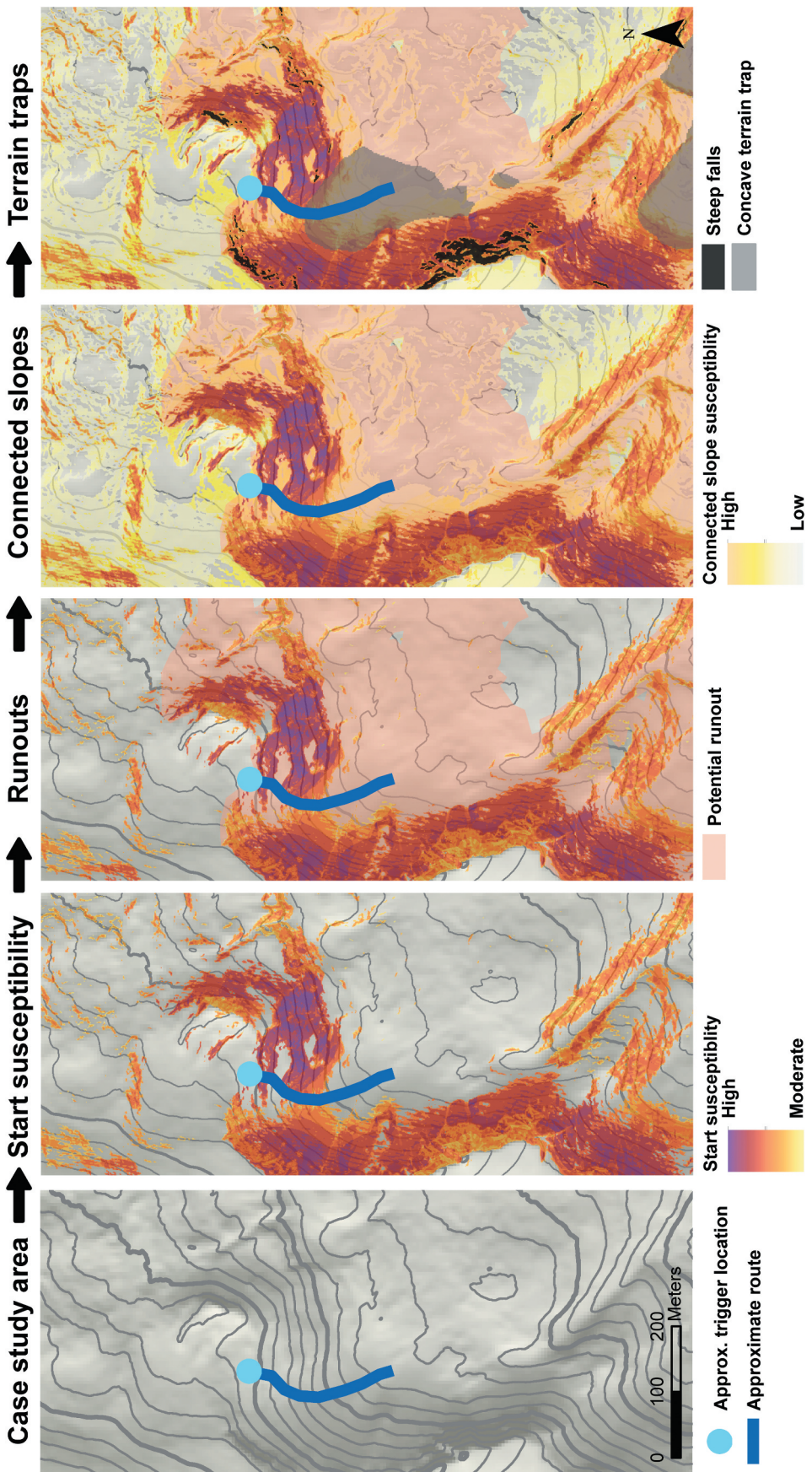
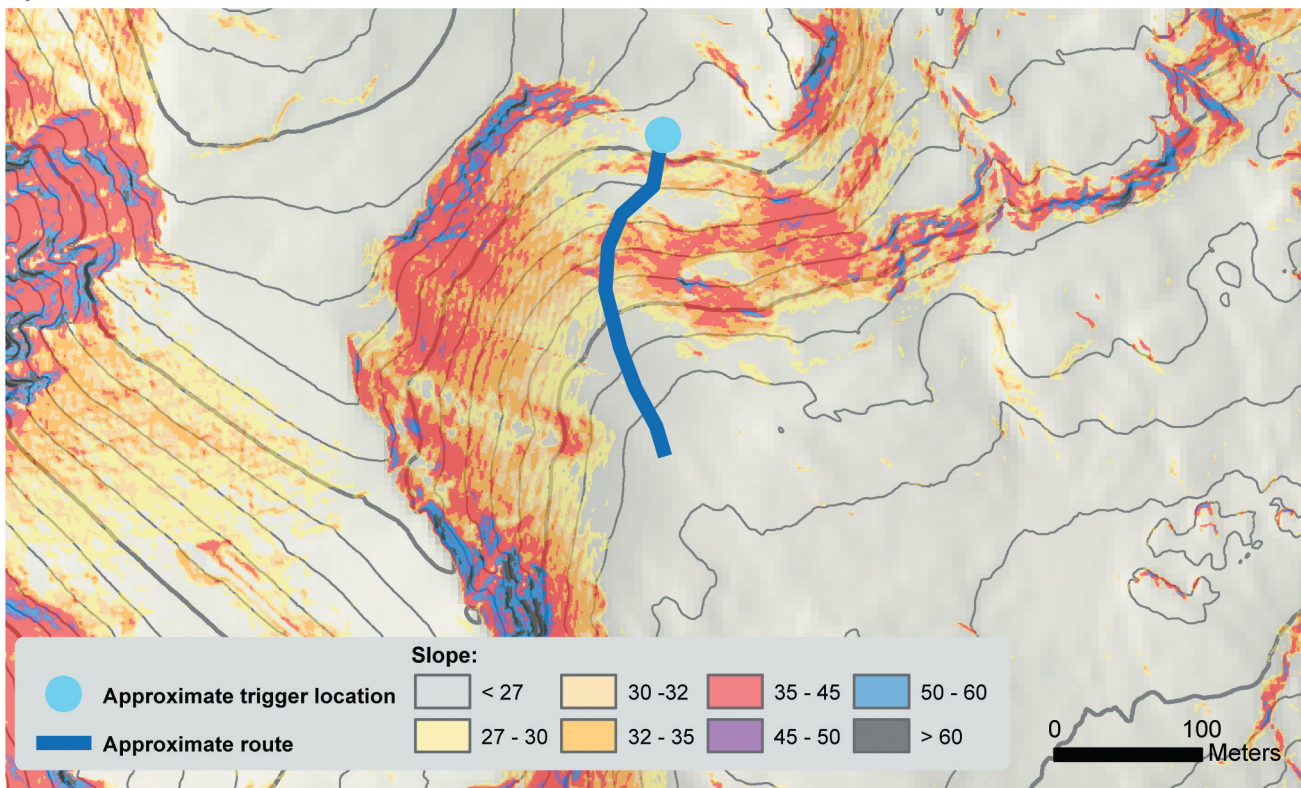


Figure 12. Progression of layers for new human-centered avalanche susceptibility mapping methodology (H-CASM) applied to the Senator Beck case study area discussed earlier in this paper. The progression starts with start zone susceptibility, then the addition of potential runouts, connected slope susceptibility, and terrain traps. The approximate trigger location (by skiers 3–6) of the initial avalanche in the case study is shown with a light blue dot. The approximate route (of skiers 1 and 2) is shown with a darker blue line.

a)



b)

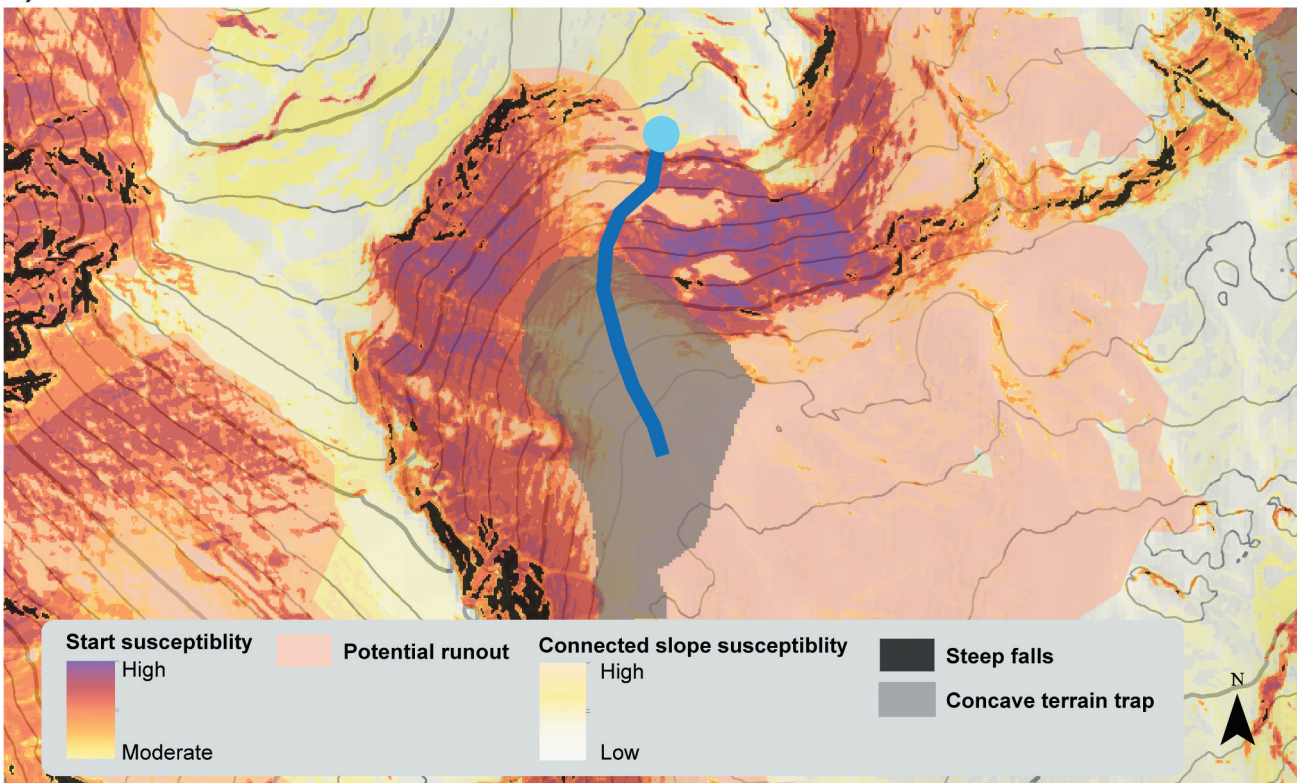


Figure 13. Comparison of a) traditional slope shading methodology and b) new human-centered avalanche susceptibility mapping methodology (H-CASM) proposed in this paper applied to the Senator Beck case study area in Red Mountain Pass, CO. The approximate trigger point by skiers 3–6 of the initial avalanche is shown with a light blue dot. The approximate route of skiers 1 and 2 is shown with a darker blue line. Notice the gray terrain trap in the H-CASM map, showing where avalanche paths may be funneled. This aligns with the case study where two avalanche paths overlapped, resulting in a fatality (skier 2).

layers can be turned on and off to optimize and individualize user experience. Much of the area appears susceptible because it is in fact susceptible. We highly encourage future work that examines how H-CASM influences risk perception.

Although Bühler et al. (2018) method for start zone delineation is the most current and accepted method, we did not utilize it. Their method requires expensive software and it is the goal of this project to create easily replicable methodology for open-source use. We have proposed a new method for the creation of start zone polygons and encourage others to test this more affordable and lower processing power methodology. We also encourage the transfer of our other processes to open-source programs. While Harvey et al. (2018) methodology is dependent on RAMMS deposition calculations, we specifically used minimal RAMMS outputs to allow for the transferability of this methodology to open-source avalanche flow algorithms.

In addition to validation, another major limitation of this study was unavailability of appropriate vegetation data. Not using a vegetation layer allowed us to model extreme scenarios with high runout distances; however, we strongly recommend it be included in future work to model higher probability slides. Raw LiDAR point cloud data are available through USGS; however, they have not been classified and requires a large amount of processing power and time. National Agriculture Imagery Program (NAIP) imagery could be used; however, studies have found classification difficult with shadows in mountainous areas (Kumar et al., 2019). The National Land Cover Database (NLCD) is of 30 m resolution, and therefore not fine enough for this analysis which was performed at 1 m (susceptibility layers) and 5 m (RAMMS runouts) resolutions. While out of the scope of this project, including vegetation density would increase the applicability of H-CASM, especially in modeling human triggered avalanches.

Finally, the public version of RAMMS is intended for detailed evaluation of a couple of avalanche paths, not iterative widespread use. This posed a major issue for this project. It is suggested that in the future, researchers either partner with Swiss Federal Institute for Forest, Snow, and Landscape Research's (WSL) Institute for Snow and Avalanche Research (SLF) to use their internal RAMMS:EXTENDED for large-scale mapping, or a simpler runout evaluation analysis with less necessary processing. It is also strongly suggested that runout calculations be re-run with more probable and less extreme scenarios to identify the most susceptible areas.

There is inherent uncertainty associated with every step of this process. Starting with the DEM, there will always be some variation between the actual environment and digital representation of it. While we did use the best resolution DEM available (one meter), one should still expect to see discrepancies. Multi-resolution modeling could be beneficial to incorporate in the future to blend contributions of fine and coarse terrain representations. We conducted field measurements of slope using a BCA inclinometer and aspect using a Sunto Compass in Wolf Creek, CO to compare traditional manual field measurements to computer generated layers (Table 7). While some measurements agree relatively well, others display more variation. This is not to say human or DEM measurements are more accurate, but that there will always be differences between computer generated and manual measurements, further confirming the need to account for uncertainty in calculations. Of the topographic variables used, Gillin et al. (2015) found the highest inconsistency between slope field and LiDAR generated DEM measurements.

Additional sources of uncertainty include start zone delineation, susceptibility weighting, and runout modeling. We attempted to reduce uncertainty within the start zone delineation by making a grid of overlapping

Table 7. Table showing comparison of manual field measurements and DEM sourced values for slope and aspect in Wolf Creek, CO.

Name	Field Slope	DEM Slope	Field Aspect	DEM Aspect
1	24	27	ENE	ENE
2	20	19	E	ESE
3	33	33	E	ESE
4	18	14	NE	ESE
5	28	24	E	NE
6	12	14	NE	E
7	40	44	NE	ENE
8	25	24	NNE	NE
9	22	18	NNW	N
10	20	22	NE	NNE
11	25	23	NE	ENE
12	36	22	N	NE
13	45	53	N	NNE
14	33	36	E	ESE

possible start zones to cover the vast majority of likely starts. Susceptibility weighting was based off an extensive literature review and expert knowledge, however, there was disagreement among sources for most influential parameters and categories (Table 1). While MCDA and AHP are commonly used and accepted methodologies, expert judgment always holds bias. We chose these methods because the focus of this paper is on creating a framework for a new approach to avalanche susceptibility mapping and not precise weighting of parameters. Fuzzy frequency or machine learning methodologies could improve the weighting process in the future. Finally, modeling runouts carries a lot of uncertainty. We tried to mitigate this as much as possible by using a well-validated model, average start depth, many start zones, and extreme scenarios for return periods by excluding vegetation. While there will always be uncertainty involved in modeling procedures, we took steps to reduce this. It is highly recommended that future work includes the quantification of these changes in uncertainty. All this said, when referring to risk maps, Monmonier (1997) stresses that “uncertainty is not an excuse for ignorance.” Put more diplomatically, while there is uncertainty involved throughout the entire map making process, we believe these maps provide invaluable information that should not be overlooked. All risk (or susceptibility) maps are partially rhetorical and carry bias and uncertainty, however they can also play an important role in increasing awareness of one’s environment and associated hazards (Monmonier, 1997).

Conclusion

We developed H-CASM, an automated, open source, and freely accessible method to create avalanche start zone susceptibility, connected slope susceptibility, terrain trap, and start zone polygon layers that can be run in an avalanche runout model to get possible runout zones. This methodology can be applied anywhere with high-resolution DEMs. We suggested cartographic design criteria for the incorporation of these outputs into a final avalanche susceptibility map that focuses on risk to humans. While there are areas for improvement within the methodology, this project serves as a proof of concept and first step in creating comprehensive human-centered avalanche susceptibility maps.

Suggested areas for future research to improve H-CASM include the following:

- (1) It is important to understand how these maps influence people’s perception of risk. More

research should be performed on this matter. Specifically, it would be beneficial to conduct interviews and scenarios with a variety of back-country recreationalists and professionals, comparing their risk perception of avalanche danger and route planning between H-CASM and traditional slope shading maps.

- (2) Incorporating vegetation density data into start zone susceptibility could be highly beneficial. Coniferous trees that are 500–1000 trees per hectare can hinder avalanche formation (Barbolini et al., 2011). With available data, this would be a valuable addition to the start zone susceptibility layer.
- (3) Aspect and VRM are dynamic topographical variables used in this study. Susceptibility maps would benefit from the incorporation of real-time wind and temperature, or official forecast site data, to influence aspect weights. Additionally weather station snow depth data could be incorporated to influence VRM, following a similar methodology to Veitinger et al. (2016).
- (4) Expert knowledge was used for start zone weighting. While this is a common and acceptable method, the process would benefit from probabilistic Bayesian networks (Grêt-Regamey & Straub, 2006) or fuzzy frequency analysis methods (Kumar et al., 2016, Veitinger et al., 2016).
- (5) We used extreme scenarios for runouts and start zone size. Performing further analysis with higher probability scenarios and representing higher probability runouts with darker shading would be beneficial.
- (6) While some validation was performed, this new method of mapping requires more validation. It would also be beneficial to perform further study and analysis in maritime and inter-mountain/transitional climatic snow zones. This analysis was performed in the southern Rocky Mountains which lie in a continental climatic zone having different characteristics from the others (McClung & Schaerer, 2006).
- (7) This methodology utilized ESRI software and RAMMS, both programs that require subscriptions and payment. It would be beneficial to transfer scripts and methodologies to open-source platforms to ensure widespread applicability.

Although digital maps can prove to be an invaluable source for people planning winter backcountry trips, it should be stressed that they are just one tool in a quiver

of resources a person should access when entering the backcountry. Recreationalists should take avalanche classes, check the weather, check the forecast, know where they are going, travel in a group, have appropriate safety gear, and be properly trained in all aspects of avalanche safety. Maps are a representation of reality and should not be solely relied upon; however, it is the responsibility of map makers to provide as detailed and accurate information as possible. This project suggests a new approach to inform the winter backcountry recreation community and their map needs.

Acknowledgments

The authors gratefully acknowledge the funding support from the American Association of Geographers Cartography Specialty Group (Master's Thesis Research Grant). We appreciate SLF's student use RAMMS-free license and Mike Cooperstein of the Colorado Avalanche Information Center for the valuable historic avalanche and weather data. The authors would also like to acknowledge Chris Lippitt and Ryan Webb for feedback on the research and manuscript, as well as Aaron Rice, John Wheeler, and Matthew Krebs for their assistance throughout the project.

Disclosure statement

No potential conflict of interest was reported by the author(s).

Funding

LLR received funding from the American Association of Geographers Cartography Specialty Group "Master's Thesis Research Grant" awarded in 2021.

Data availability statement

Codes discussed in this paper are available at <https://github.com/lrotche/AvalancheSusceptibility>. Final layers used in the map figures in this paper are available at https://figshare.com/articles/dataset/RotcheLin_DataLayers_zip/22064537. All DEMs were acquired through USGS's publicly available 3DEP dataset. Historic avalanche and weather data were provided through CAIC. We do not have permission to publish those datasets.

References

- American Avalanche Association. (2021). *US Avalanche Fatalities*. <https://avalanche.org/avalanche-accidents/>
- Andres, A. J., & Cr'a, J. C. (2012). Mapping of avalanche start zones susceptibility: Arazas basin, Ordesa and Monte Perdido National Park (Spanish pyrenees). *Journal of Maps*, 8(1), 14–21. <https://doi.org/10.1080/17445647.2012.668414>
- Aydin, A., & Eker, R. (2017). GIS-based snow avalanche hazard mapping: Bayburt-Aşağı Dere catchment case. *Journal of Environmental Biology*, 38(5(SI)), 937–943. [https://doi.org/10.22438/jeb/38/5\(SI\)/GM-10](https://doi.org/10.22438/jeb/38/5(SI)/GM-10)
- Barbolini, M., Pagliardi, M., Ferro, F., & Corradeghini, P. (2011). Avalanche hazard mapping over large undocumented areas. *Natural Hazards*, 56(2), 451–464. <https://doi.org/10.1007/s11069-009-9434-8>
- Bergua, S. B., Poblete Piedrabuena, M. Á., & Marino Alfonso, J. L. (2018). Snow avalanche susceptibility in the eastern hillside of the aramo range (Asturian central Massif, cantabrian mountains, NW Spain). *Journal of Maps*, 14(2), 373–381. <https://doi.org/10.1080/17445647.2018.1480974>
- Brassel, K. E., & Utano, J. J. (1979). Design strategies for continuous-tone area mapping. *The American Cartographer*, 6(1), 39–50. <https://doi.org/10.1559/152304079784022718>
- Bühler, Y., Bebi, P., Christen, M., Margreth, S., Stoffel, L., Stoffel, A., Marty, C., Schmucki, G., Caviezel, A., Kühne, R., Wohlwend, S., & Bartelt, P. (2022). Automated avalanche hazard indication mapping on state wide scale. *Natural Hazards and Earth System Sciences*, 22(6), 1825–1843. <https://doi.org/10.5194/nhess-2022-11>
- Bühler, Y., Kumar, S., Veitinger, J., Christen, M., Stoffel, A., & Snehmani. (2013). Automated identification of potential snow avalanche release areas based on digital elevation models. *Natural Hazards and Earth System Sciences*, 13(5), 1321–1335. <https://doi.org/10.5194/nhess-13-1321-2013>
- Bühler, Y., von Rickenbach, D., Stoffel, A., Margreth, S., Stoffel, L., & Christen, M. (2018). Automated snow avalanche release area delineation – validation of existing algorithms and proposition of a new object-based approach for large-scale hazard indication mapping. *Natural Hazards and Earth System Sciences*, 18(12), 3235–3251. <https://doi.org/10.5194/nhess-18-3235-2018>
- CAIC. (2021). *Historic avalanche data*. Unpublished Raw Data.
- CAIC. (2022). *Abrahms weather station data*. Unpublished Raw Data.
- Choubin, B., Borji, M., Mosavi, A., Sajedi-Hosseini, F., Singh, V. P., & Shamshirband, S. (2019). Snow avalanche hazard prediction using machine learning methods. *Canadian Journal of Fisheries and Aquatic Sciences*, 577, 123929. <https://doi.org/10.1016/j.jhydrol.2019.123929>
- Christen, M., Kowalski, J., & Bartelt, P. (2010). RAMMS: Numerical simulation of dense snow avalanches in three-dimensional terrain. *Cold Regions Science and Technology*, 63(1–2), 1–14. <https://doi.org/10.1016/j.coldregions.2010.04.005>
- Chyomyrov, A., Zeidler, A., Perzl, F., & Nazarkulov, K. (2019). The avalanche geodatabase development and hazard mapping for the Bishkek-Osh road in Kyrgyzstan. *International Journal of Geoinformatics*, 15(4), 19–27.
- Cía, J. C., Andrés, A. J., & Montañés Magallón, A. (2014). A proposal for avalanche susceptibility mapping in the pyrenees using GIS: The Formigal-Peyreget area (Sheet 145-I; scale 1: 25.000). *Journal of Maps*, 10(2), 203–210. <https://doi.org/10.1080/17445647.2013.870501>
- Dewali, S. K., Joshi, J. C., Ganju, A., & Snehmani. (2014). A GPS-based real-time avalanche path warning and navigation system. *Geomatics, Natural Hazards and Risk*, 5(1), 56–80. <https://doi.org/10.1080/19475705.2012.762429>
- Gasson, S. (2003). Human-centered vs. user-centered approaches to information system design. *The Journal of*

- Information Technology Theory and Application*, 5(2), 29–46. <https://aisel.aisnet.org/jitta/vol5/iss2/5/>
- Ghinoi, A., & Chung, C.-J. (2005). STARTER: A statistical GIS-based model for the prediction of snow avalanche susceptibility using terrain features—application to alta val badia, Italian Dolomites. *Geomorphology*, 66(1–4), 305–325. <https://doi.org/10.1016/j.geomorph.2004.09.018>
- Gillin, C. P., Bailey, S. W., McGuire, K. J., & Prisley, S. P. (2015). Evaluation of lidar-derived DEMs through terrain analysis and field comparison. *Photogrammetric Engineering & Remote Sensing*, 81(5), 387–396. <https://doi.org/10.14358/PERS.81.5.387>
- Greene, E., Davis, J., Mellick, A., & Bilbrey, C. (2019). 2019/01/05—Colorado—upper senator beck basin, northwest of red mountain pass [CAIC]. https://avalanche.state.co.us/caic/acc/acc_report.php?accfm=inv&acc_id=685
- Grêt-Regamey, A., & Straub, D. (2006). Spatially explicit avalanche risk assessment linking Bayesian networks to a GIS. *Natural Hazards and Earth System Sciences*, 6(6), 911–926. <https://doaj.org/article/fc00f09b819247d5a209a9deaa05e8d5>
- Gruber, U. S., & Sardemann, S. (2003). High-frequency avalanches: Release area characteristics and run-out distances. *Cold Regions Science and Technology*, 37(3), 439–451. [https://doi.org/10.1016/S0165-232X\(03\)00083-1](https://doi.org/10.1016/S0165-232X(03)00083-1)
- Gusain, H. S., Negi, H. S., Dhamija, S., Mishra, V. D., & Snehmani. (2019). Development of avalanche information system using remote sensing and GIS technology in the Indian Karakoram Himalaya. *Current Science*, 117(1), 104. <https://doi.org/10.18520/cs/v117/i1/104-109>
- Harvey, S., Schmudlach, G., Bühler, Y., Dürr, L., Stoffel, A., & Christen, M. (2018). Avalanche terrain maps for backcountry skiing in Switzerland. *International Snow Science Workshop ISSW, Innsbruck, Austria*.
- Hoarau, C. (2011). Reaching a compromise between contextual constraints and cartographic rules: Application to sustainable maps. *Cartography and Geographic Information Science*, 38(2), 79–88. <https://doi.org/10.1559/1523040638279>
- Kim, S.-M., & Park, H.-D. (2019). Analogy between grid-based modeling of landslide and avalanche using GIS with surface flow analysis. *Bulletin of Engineering Geology and the Environment*, 78(1), 189–206. <https://doi.org/10.1007/s10064-017-1144-y>
- Kumar, S., Srivastava, P. K., Gore, A., & Singh, M. K. (2016). Fuzzy-frequency ratio model for avalanche susceptibility mapping. *International Journal of Digital Earth*, 9(12), 1168–1184. <https://doi.org/10.1080/17538947.2016.1197328>
- Kumar, S., Srivastava, P. K., & Snehmani. (2018). Geospatial modelling and mapping of snow avalanche susceptibility. *The Journal of the Indian Society of Remote Sensing*, 46(1), 109–119. <https://doi.org/10.1007/s12524-017-0672-z>
- Kumar, S., Srivastava, P. K., Snehmani, & Bhatiya, S. (2019). Geospatial probabilistic modelling for release area mapping of snow avalanches. *Cold Regions Science & Technology*, 165, 102813. <https://doi.org/10.1016/j.coldregions.2019.102813>
- Kunz, M., Grêt-Regamey, A., & Hurni, L. (2011). Customized visualization of natural hazards assessment results and associated uncertainties through interactive functionality. *Cartography and Geographic Information Science*, 38(2), 232–242. <https://doi.org/10.1559/15230406382232>
- Larsen, H. T., Hendrikx, J., Slåtten, M. S., & Engeset, R. V. (2020). Developing nationwide avalanche terrain maps for Norway. *Natural Hazards*, 103(3), 2829–2847. <https://doi.org/10.1007/s11069-020-04104-7>
- Laute, K., & Beylich, A. A. (2014). Morphometric and meteorological controls on recent snow avalanche distribution and activity at hillslopes in steep mountain valleys in western Norway. *Geomorphology*, 218, 16–34. <https://doi.org/10.1016/j.geomorph.2013.06.006>
- Maggioni, M., & Gruber, U. (2003). The influence of topographic parameters on avalanche release dimension and frequency. *Cold Regions Science and Technology*, 37(3), 407–419. [https://doi.org/10.1016/S0165-232X\(03\)00080-6](https://doi.org/10.1016/S0165-232X(03)00080-6)
- McClung, D., & Schaerer, P. (2006). *The avalanche handbook* (3rd ed.). The Mountaineers Books.
- Mohammed, A. A., Naqvi, H. R., & Firdouse, Z. (2015). An assessment and identification of avalanche hazard sites in Uri sector and its surroundings on Himalayan mountain. *Journal of Mountain Science*, 12(6), 1499–1510. <https://doi.org/10.1007/s11629-014-3274-z>
- Monmonier, M. S. (1997). *Cartographies of danger: Mapping hazards in America*. University of Chicago Press.
- Özşahin, E., & Kaymaz, Ç. K. (2014). Avalanche susceptibility and risk analysis of eastern Anatolian region using GIS. *Procedia - Social & Behavioral Sciences*, 120, 663–672. <https://doi.org/10.1016/j.sbspro.2014.02.147>
- Parshad, R., Srivastva, P. K., Snehmani, Ganguly, S., Kumar, A., & Ganju, A. (2017). Snow avalanche susceptibility mapping using remote sensing and GIS in Nubra-Shyok Basin, Himalaya, India. *Indian Journal of Science & Technology*, 10(31). <https://doi.org/10.17485/ijst/2017/v10i31/105647>
- Pistocchi, A., & Notarnicola, C. (2013). Data-driven mapping of avalanche release areas: A case study in South Tyrol, Italy. *Natural Hazards*, 65(3), 1313–1330. <https://doi.org/10.1007/s11069-012-0410-3>
- Raisz, E. (1962). *Principles of Cartography*. McGraw-Hill Book Company.
- Robinson, A., & Sale, R. (1969). *Elements of Cartography* (3rd ed.). John Wiley & Sons, Inc.
- Rotche, L. (2022). *AvalancheSusceptibility*. <https://github.com/lrotche/AvalnacheSusceptibility>
- Sappington, J. M., Longshore, K. M., & Thompson, D. B. (2007). Quantifying landscape ruggedness for animal habitat analysis: A case study using bighorn sheep in the Mojave Desert. *The Journal of Wildlife Management*, 71(5), 1419–1426. <https://doi.org/10.2193/2005-723>
- Schmudlach, G., & Köhler, J. (2016). *Method for an automated avalanche terrain classification* [Proceedings]. International Snow Science Workshop, Breckenridge, Colorado.
- Selcuk, L. (2013). An avalanche hazard model for Bitlis Province, Turkey, using GIS based multicriteria decision analysis. *Turkish Journal of Earth Sciences*, 22, 523–535. <https://doi.org/10.3906/yer-1201-10>
- Silverton Chamber of Commerce. (2022). *A year-round destination in the heart of the high country*. <https://www.silvertoncolorado.com/>
- SLF. (2022). *Long-Term Statistics*. <https://www.slf.ch/en/avalanches/destructive-avalanches-and-avalanche-accidents/long-term-statistics.html>

- Soteres, R. L., Pedraza, J., & Carrasco, R. M. (2020). Snow avalanche susceptibility of the Circo de Gredos (Iberian central system, Spain). *Journal of Maps*, 16(2), 155–165. <https://doi.org/10.1080/17445647.2020.1717655>
- Strapazzon, G., Schweizer, J., Chiambretti, I., Brodmann Maeder, M., Brugger, H., & Zafren, K. (2021). Effects of climate change on avalanche accidents and survival. *Frontiers in Physiology*, 12, 639433. <https://doi.org/10.3389/fphys.2021.639433>
- Suk, P., & Klimánek, M. (2011). Creation of the snow avalanche susceptibility map of the Krkonoše Mountains using GIS. *Acta Universitatis Agriculturae et Silviculturae Mendelianae Brunensis*, 59(5), 237–246. <https://doi.org/10.11118/actaun201159050237>
- Sun, S. (2015). A perception-based color recommendation algorithm for hierarchical regions. *Cartography and Geographic Information Science*, 42(3), 259–270. <https://doi.org/10.1080/15230406.2014.991424>
- Sykes, J., Haegeli, P., & Bühler, Y. (2021). *Automated snow avalanche release area delineation in data sparse, remote, and forested regions*. [Preprint]. Other Hazards (e.g., Glacial and Snow Hazards, Karst, Wildfires Hazards, and Medical Geo-Hazards). <https://doi.org/10.5194/nhess-2021-330>
- Tariq, S., Abdur, R., Abdur, R., & Ghulam, S. (2019). Snow avalanche based susceptibility assessment of selected districts in northern zone of Pakistan applying MCDA approach in GIS. *Journal of Himalayan Earth Sciences*, 52(2), 67–73.
- Temper, B. (2008). *Staying alive in avalanche terrain* (Secong). The Mountaineers Books.
- USGS. (2022). *3D elevation program 1-meter resolution digital elevation models*. United States Geological Survey. <https://apps.nationalmap.gov/downloader/>
- Veitinger, J., Purves, R. S., & Sovilla, B. (2016). Potential slab avalanche release area identification from estimated winter terrain: A multi-scale, fuzzy logic approach. *Natural Hazards and Earth System Sciences*, 16(10), 2211–2225. <https://doi.org/10.5194/nhess-16-2211-2016>
- Vontobel, I., Harvey, S., & Purves, R. (2013). Terrain analysis of skier-triggered avalanche starting zones. *International Snow Science Workshop Grenoble – Chamonix Mont-Blanc*.
- Weiss, A. D. (2001). *Topographic position and landforms analysis* [Poster presentation]. ESRI User's Conference, San Diego, CA.
- Yariyan, P., Avand, M., Abbaspour, R. A., Karami, M., & Tiefenbacher, J. P. (2020). GIS-based spatial modeling of snow avalanches using four novel ensemble models. *Science of the Total Environment*, 745, 141008. <https://doi.org/10.1016/j.scitotenv.2020.141008>